10
Neutrino detectors

Neutrino physics is largely an art of learning a great deal by observing nothing.

Haim Harari

10.1 Neutrino sources

The detection of neutrinos is a challenge. Due to the smallness of neutrino interaction cross sections, neutrino detectors are required to be very massive to provide measurable rates. The cross section for neutrino–nucleon scattering of 10 GeV neutrinos is on the order of $7 \cdot 10^{-38}\,\mathrm{cm}^2$/nucleon. Thus, for a target of 10 m of solid iron the interaction probability

$$R = \sigma \cdot N_\mathrm{A}\,[\mathrm{mol}^{-1}]/\mathrm{g} \cdot d \cdot \varrho \tag{10.1}$$

(σ – nuclear cross section, N_A – Avogadro's number, d – target thickness, ϱ – density) is only

$$R = 7 \cdot 10^{-38}\,\mathrm{cm}^2 \cdot 6.023 \cdot 10^{23}\,\mathrm{g}^{-1} \cdot 10^3\,\mathrm{cm} \cdot 7.6\,\frac{\mathrm{g}}{\mathrm{cm}^3} = 3.2 \cdot 10^{-10}\ . \tag{10.2}$$

Therefore, it is very unlikely that neutrinos interact even in a massive detector. The situation is even worse for low-energy neutrinos. Solar neutrinos of 100 keV are associated with a cross section for neutrino–nucleon scattering of

$$\sigma(\nu_e N) \approx 10^{-45}\,\mathrm{cm}^2/\mathrm{nucleon}\ . \tag{10.3}$$

The interaction probability of these neutrinos with our planet Earth at a central collision is only $\approx 4{\cdot}10^{-12}$. In addition to low cross sections threshold effects also play an important rôle. Energies in the several 100 keV range are below the threshold for inverse β decay ($\bar{\nu}_e + p \rightarrow n + e^+$),

https://doi.org/10.1017/9781009401531.013 Published online by Cambridge University Press

where a minimum antineutrino energy of 1.8 MeV is required to induce this reaction. To get measurable interaction rates therefore high neutrino fluxes and not too low energies are necessary.

Neutrinos are generated in *weak interactions* and decays [1–3]. Reactor neutrinos originate from nuclear β decay,

$$n \rightarrow p + e^- + \bar{\nu}_e \quad (\beta^- \text{ decay}) \ , \tag{10.4}$$

$$p \rightarrow n + e^+ + \nu_e \quad (\beta^+ \text{ decay}) \ , \tag{10.5}$$

$$p + e^- \rightarrow n + \nu_e \quad (\text{electron capture}) \ . \tag{10.6}$$

These neutrinos have typically MeV energies.

Stars produce energy by nuclear fusion, creating only electron-type neutrinos, mostly via proton–proton fusion

$$p + p \rightarrow d + e^+ + \nu_e \ , \tag{10.7}$$

but also in electron-capture reactions with ^{7}Be,

$$^7\text{Be} + e^- \rightarrow {}^7\text{Li} + \nu_e \tag{10.8}$$

and decays from boron,

$$^8\text{B} \rightarrow {}^8\text{Be} + e^+ + \nu_e \ . \tag{10.9}$$

Solar neutrinos range from the keV region to about 15 MeV.

Neutrinos are also copiously produced in the atmosphere in air showers initiated by primary cosmic-ray nuclei where mainly pions and kaons are the parents of muon neutrinos,

$$\pi^+ \rightarrow \mu^+ + \nu_\mu \ , \tag{10.10}$$

$$\pi^- \rightarrow \mu^- + \bar{\nu}_\mu \ , \tag{10.11}$$

$$K^+ \rightarrow \mu^+ + \nu_\mu \ , \tag{10.12}$$

$$K^- \rightarrow \mu^- + \bar{\nu}_\mu \ . \tag{10.13}$$

The decay of muons yields also electron-type neutrinos,

$$\mu^+ \rightarrow e^+ + \nu_e + \bar{\nu}_\mu \ , \tag{10.14}$$

$$\mu^- \rightarrow e^- + \bar{\nu}_e + \nu_\mu \ . \tag{10.15}$$

Atmospheric neutrinos can be very energetic ($\geq$ GeV).

Supernova explosions are a strong source of neutrinos. These neutrinos can originate from the deleptonisation phase where protons and electrons are merged,

$$p + e^- \rightarrow n + \nu_e \ , \tag{10.16}$$

https://doi.org/10.1017/9781009401531.013 Published online by Cambridge University Press

producing only electron neutrinos, while all neutrino flavours are democratically generated via weak decays of virtual Zs made in e^+e^- interactions,

$$e^+e^- \;\to\; Z \;\to\; \nu_\alpha + \bar{\nu}_\alpha \quad (\alpha = e, \mu, \tau) \;. \tag{10.17}$$

High-energy neutrinos can be obtained from earthbound or cosmic accelerators in *beam-dump experiments*, where they are created in weak decays of short-lived hadrons. The total cross section for high-energy neutrinos rises linearly with energy until propagator effects from Z or W exchange saturate the cross section.

Finally, the Big Bang was a rich source of neutrinos which have cooled down during the expansion of the universe to a present temperature of 1.9 K, corresponding to $\approx 0.16\,\mathrm{MeV}$ [4, 5].

10.2 Neutrino reactions

Neutrinos can be detected in weak interactions with nucleons. There are characteristic *charged-current interactions* for the different neutrino flavours,

$$\nu_e + n \to e^- + p \;, \tag{10.18}$$
$$\bar{\nu}_e + p \to e^+ + n \;, \tag{10.19}$$
$$\nu_\mu + n \to \mu^- + p \;, \tag{10.20}$$
$$\bar{\nu}_\mu + p \to \mu^+ + n \;, \tag{10.21}$$
$$\nu_\tau + n \to \tau^- + p \;, \tag{10.22}$$
$$\bar{\nu}_\tau + p \to \tau^+ + n \;. \tag{10.23}$$

The corresponding *neutral-current interactions* are not very helpful for neutrino detection since a large fraction of the energy is carried away by the final-state neutrino.

However, neutrinos can also be detected in neutral-current interactions with atomic electrons,

$$\nu_\alpha + e^- \;\to\; \nu_\alpha + e^- \quad (\alpha = e, \mu, \tau) \;, \tag{10.24}$$

where a fraction of the neutrino energy is transferred to the final-state electron, which can be measured. For antineutrinos such reactions are also possible, with the speciality that in $\bar{\nu}_e e^-$ scattering – if the centre-of-mass energy is sufficiently high – also muons and taus can be produced,

$$\bar{\nu}_e + e^- \to \mu^- + \bar{\nu}_\mu \;, \tag{10.25}$$
$$\bar{\nu}_e + e^- \to \tau^- + \bar{\nu}_\tau \;. \tag{10.26}$$

https://doi.org/10.1017/9781009401531.013 Published online by Cambridge University Press

As already indicated, the cross sections for the different neutrino interactions are very small, in particular, for low-energy neutrinos. To circumvent this problem, the missing-energy or missing-momentum technique has been invented in elementary particle physics experiments, where the neutrino flavour and its four-momentum are inferred from the particles seen in the detector. This procedure requires the knowledge of the available energy for the reaction. If, e.g., a W pair is produced in e^+e^- collisions,

$$e^+ + e^- \;\rightarrow\; W^+ + W^- \;, \tag{10.27}$$

where one W decays hadronically ($W^- \rightarrow u\bar{d}$) and the other leptonically ($W^+ \rightarrow \mu^+ + \bar{\nu}_\mu$), the energy and momentum of the $\bar{\nu}_\mu$ can be inferred from the four-momenta of all visible particles if the centre-of-mass energy of the collision is known. The flavour of the neutrino is obvious from the generated muon.

10.3 Some historical remarks on neutrino detection

Cowan and Reines [6] discovered the $\bar{\nu}_e$ in the 1950s via the reaction

$$\bar{\nu}_e + p \;\rightarrow\; e^+ + n \;, \tag{10.28}$$

where the positron was identified in the annihilation process

$$e^+ + e^- \;\rightarrow\; \gamma + \gamma \tag{10.29}$$

yielding two back-to-back photons of 511 keV each in delayed coincidence with photons originating from the γ decay of an excited nucleus after neutron capture. The neutrino detector used in this 'Poltergeist' experiment consisted of a large liquid-scintillation counter.

Muon neutrinos as distinct from electron neutrinos were first seen in the famous 'two-neutrino experiment' by Lederman, Schwartz, and Steinberger [7] in 1962 through the reaction

$$\nu_\mu + n \;\rightarrow\; \mu^- + p \;, \tag{10.30}$$

where the large spark-chamber detector could easily tell muons from electrons, because muons only produce straight tracks, while electrons – if they would have been generated in such a reaction – would have initiated electromagnetic cascades (see also Chap. 16), which exhibit a distinctly different pattern in the spark-chamber stack.

https://doi.org/10.1017/9781009401531.013 Published online by Cambridge University Press

The existence of tau neutrinos was indirectly inferred from μ, e events observed in e^+e^- interactions [8],

$$\begin{aligned} e^+ + e^- \rightarrow \tau^+ + \tau^- & \\ \hookrightarrow\ e^- + \bar{\nu}_e + \nu_\tau & \\ \hookrightarrow\ \mu^+ + \nu_\mu + \bar{\nu}_\tau\ . & \end{aligned} \tag{10.31}$$

The direct observation of τ neutrinos by the DONUT experiment in the year 2000,

$$\nu_\tau + N \ \rightarrow\ \tau^- + X\ , \tag{10.32}$$

with subsequent decay of the τ^- completed the third family of leptons [9]. Due to the short lifetime of the tau this experiment required a massive but fine-grained detector of very high spatial resolution. This was achieved by a large-volume nuclear-emulsion detector which, however, required tedious scanning to find the τ-decay vertices.

10.4 Neutrino detectors

Neutrino detection is always very indirect. Neutrinos are caused to undergo interactions in which charged particles, excited nuclei or excited atoms are produced which then can be detected with standard measurement techniques. The simplest form is neutrino counting. This is the basis of radiochemical experiments in which solar neutrinos have first been detected in the chlorine experiment in the Homestake Mine [10, 11].

If the neutrino exceeds a certain threshold energy, the following reaction can occur:

$$\nu_e + {}^{37}\mathrm{Cl} \ \rightarrow\ {}^{37}\mathrm{Ar} + e^-\ , \tag{10.33}$$

where a neutron in the chlorine nucleus is transformed into a proton. The argon isotope is purged out of the detector volume and counted in a proportional counter, which has an extremely low background rate. The argon isotope undergoes electron capture,

$${}^{37}\mathrm{Ar} + e^- \ \rightarrow\ {}^{37}\mathrm{Cl} + \nu_e\ , \tag{10.34}$$

which leaves the chlorine in an excited atomic state. This in turn transforms into the ground state by the emission of characteristic X rays or Auger electrons which are eventually the evidence that a neutrino detection has occurred. The gallium experiments for solar-neutrino detection work along similar lines.

Figure 10.1 shows the proportional-tube detector for the GALLEX experiment [12], which has measured the radioactive decay of the

https://doi.org/10.1017/9781009401531.013 Published online by Cambridge University Press

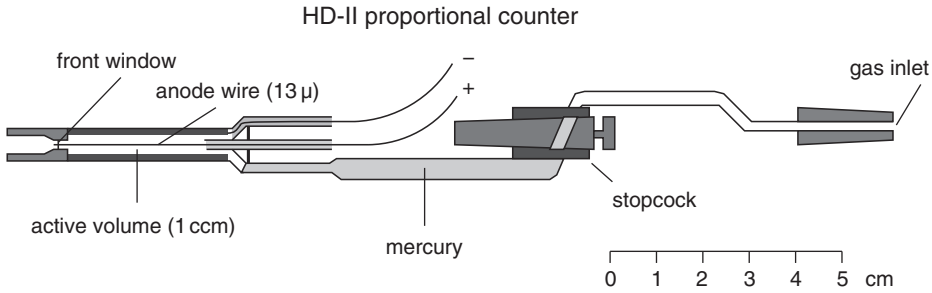

Fig. 10.1. Proportional-tube detector for the GALLEX experiment [12]; the radioactive decay of the produced ^{71}Ge is measured in a similar way as in the chlorine experiment by Ray Davis. The produced ^{71}Ge in the form of germane (GeH_4) is pressed into the proportional tube with the help of mercury. The germane (70%) is mixed with xenon (30%) to increase the photo absorption of the characteristic X rays [13].

neutrino-induced ^{71}Ge in a similar way as the ^{37}Ar was counted in the chlorine experiment by Ray Davis.

Calorimetric neutrino detectors for high-energy neutrinos are based on the measurement of the total energy of the final-state hadrons produced in a neutrino–nucleon interaction. These calorimeters are mostly sandwiches consisting of alternating passive targets and active detectors (e.g. scintillators) like those being used for hadron calorimeters. Of course, also total-absorption calorimeters can be built, where the target at the same time must be an active detector element. The large neutrino detectors at CERN (CDHS and Charm) were sampling detectors while KARMEN and SuperKamiokande are large-volume total-absorption devices exploiting Cherenkov- and scintillation-light detection. Depending on which neutrino flavour is being detected the calorimeter must be sensitive not only to hadrons but also to electrons or muons.

A photo of the sampling calorimeter used by the CDHS collaboration is shown in Fig. 10.2 [14]. The track-reconstruction capability of this experiment is demonstrated by the di-muon event as shown in Fig. 10.3 [14]. The KARMEN experiment (Fig. 10.4) is an example of a total-absorption scintillation calorimeter. The central part of the detector consists of a stainless-steel tank filled with 65 000 l of liquid scintillator. Details of the photomultiplier readout of the end faces are explained in Fig. 10.4 [15].

If the active elements in a total-absorption or sampling calorimetric system provide some spatial information, one is able to distinguish different final-state products in such neutrino tracking detectors. In reactions like

$$\nu_\mu + N \;\rightarrow\; \mu^- + \text{hadrons} \tag{10.35}$$

https://doi.org/10.1017/9781009401531.013 Published online by Cambridge University Press

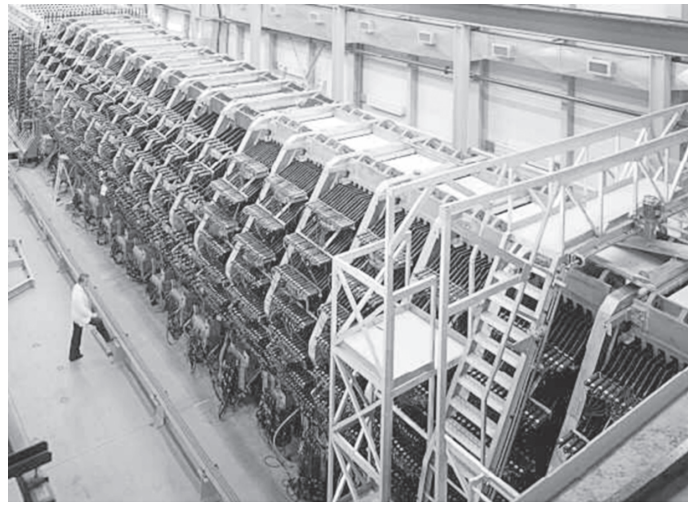

Fig. 10.2. Photo of the CDHS experiment [14].

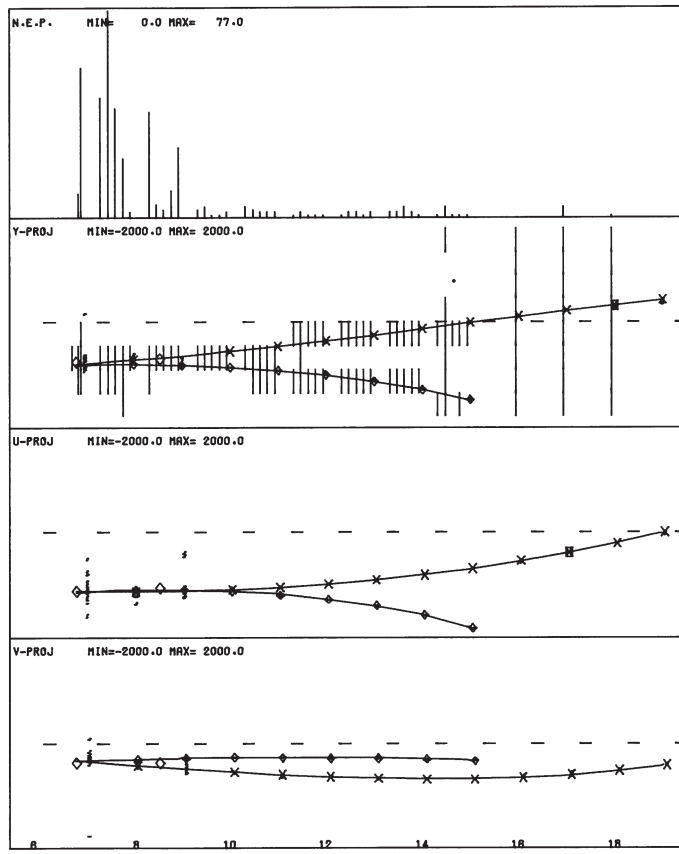

Fig. 10.3. Event display of a di-muon event in the CDHS detector [14]. In this event reconstruction the energy deposits and the muon tracks in different projections are shown.

https://doi.org/10.1017/9781009401531.013 Published online by Cambridge University Press

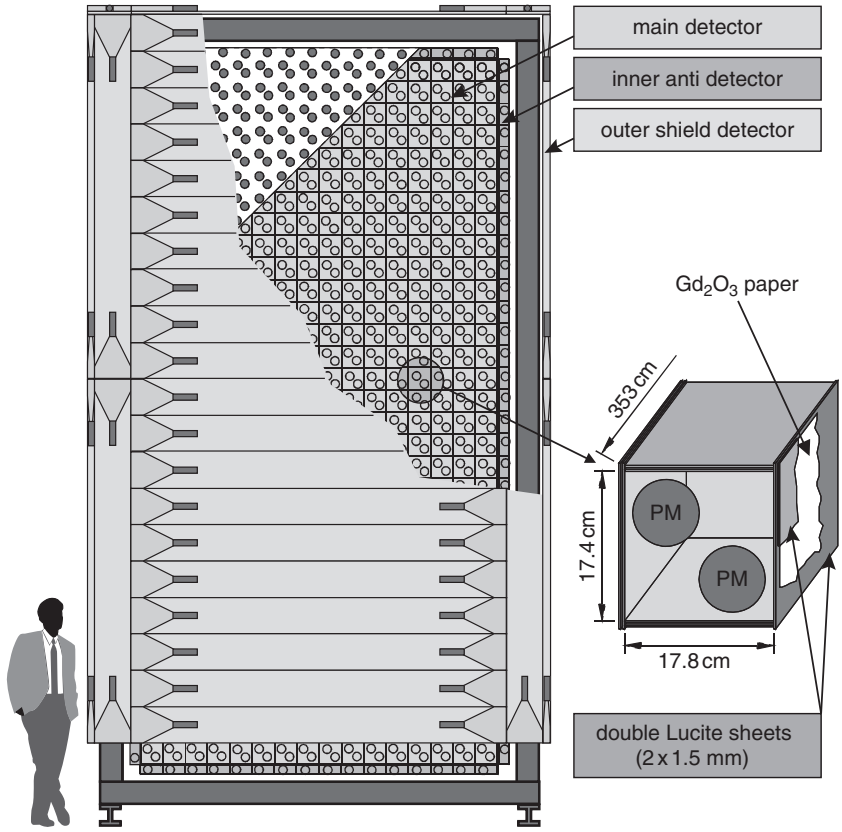

Fig. 10.4. Experimental setup of the KARMEN detector. The detector is constructed as a large-volume liquid-scintillation calorimeter. The central part of the detector consists of a stainless-steel tank filled with 65 000 l of liquid scintillator. Details of the photomultiplier readout of the end faces is shown in the lower right-hand part of the figure [15].

one identifies the muon as penetrating particle and one might be able to resolve the final-state hadrons and even determine the momentum if the tracking system is operated in a magnetic field. The NOMAD experiment (Figs. 10.5 and 10.6), just as the CDHS and Charm experiments, provides this kind of information [16].

A classical type of neutrino detector, where energy and momentum measurements are simultaneously performed, are large-volume bubble chambers with external muon identifiers. A photograph of the Big European Bubble Chamber BEBC, which is immersed in a strong magnetic field, is shown in Fig. 10.7 [17]. This bubble chamber can be filled with different liquids so that the target for interactions can be varied to the needs of the experimenter.

https://doi.org/10.1017/9781009401531.013 Published online by Cambridge University Press

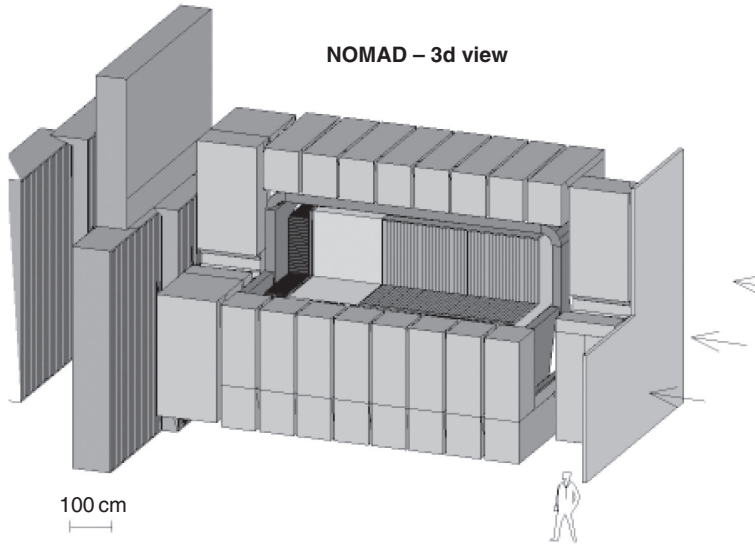

Fig. 10.5. Sketch of the NOMAD experiment [16].

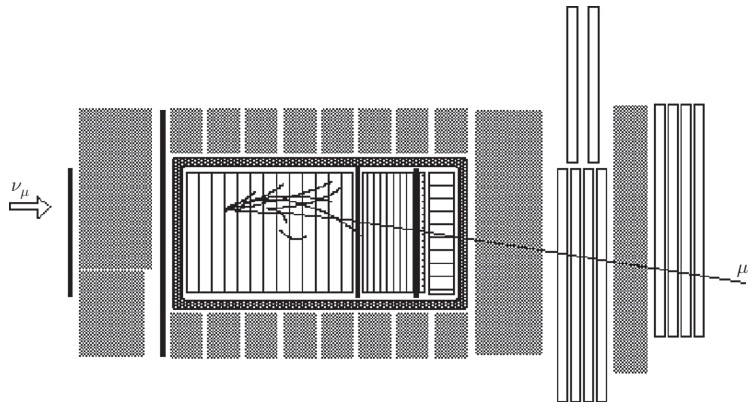

Fig. 10.6. Muon-neutrino-induced inelastic interaction in the NOMAD experiment [16].

Bubble-chamber pictures allow to obtain very detailed information on the final-state products of the neutrino interaction at the expense of a tedious scanning. Figure 10.8 shows the world's first neutrino observation in a 12-foot hydrogen bubble chamber at Argonne [18]. The invisible neutrino strikes a proton where three particle tracks originate. The neutrino turns into a muon, visible by the long track. The short track is the proton.

Figure 10.9 is an example of the rich information a bubble chamber can provide. It shows a charged-current inelastic interaction of a muon

https://doi.org/10.1017/9781009401531.013 Published online by Cambridge University Press

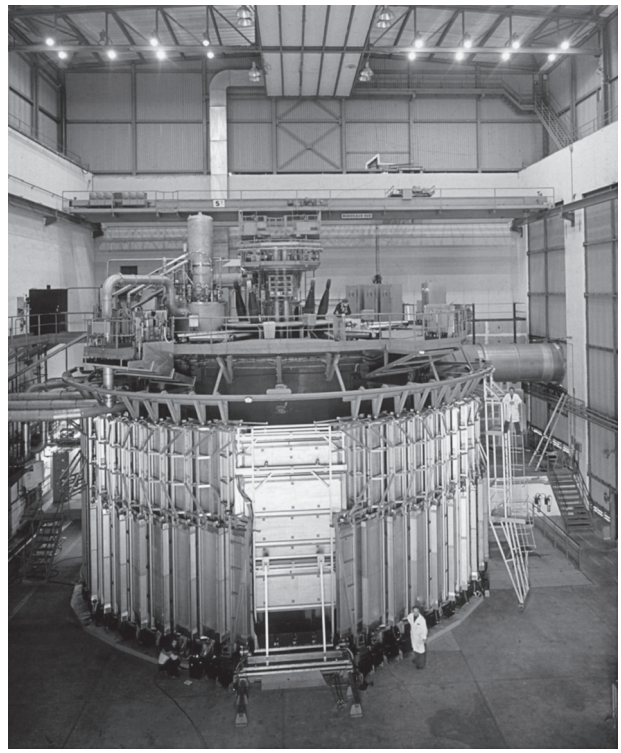

Fig. 10.7. Photo of the Big European Bubble Chamber, BEBC [17]; Photo credit CERN.

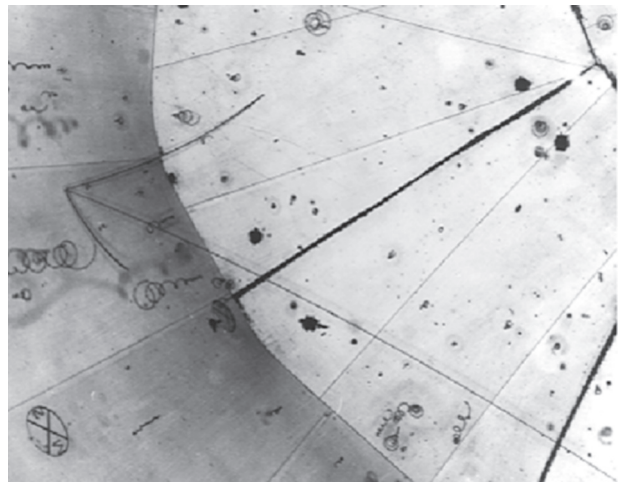

Fig. 10.8. The world's first neutrino observation in a 12-foot hydrogen bubble chamber at Argonne. The invisible neutrino strikes a proton where three particle tracks originate. The neutrino turns into a muon, the long track. The short track is the proton. The third track is a pion created by the collision; $\nu_\mu + p \rightarrow \mu^- + p + \pi^+$; Photo credit Argonne National Laboratory [18].

https://doi.org/10.1017/9781009401531.013 Published online by Cambridge University Press

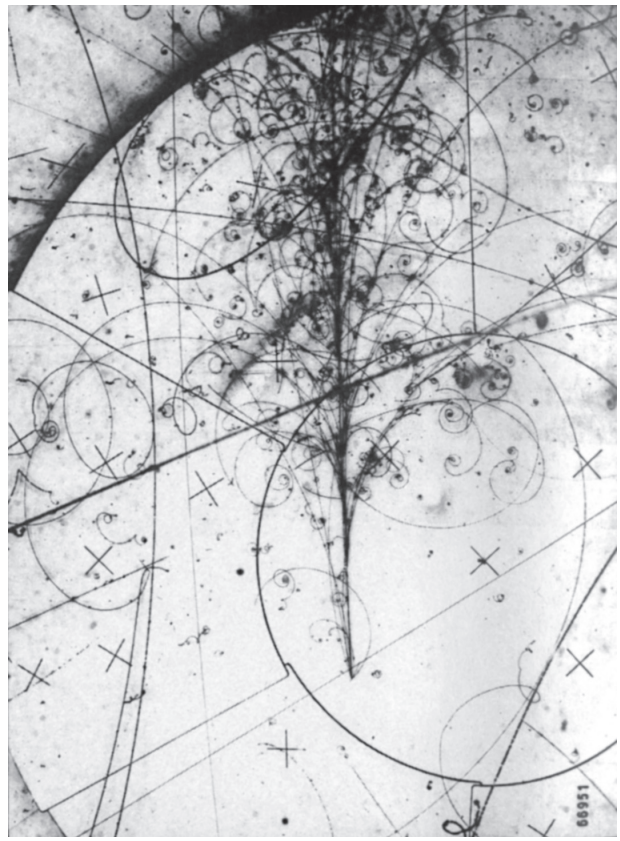

Fig. 10.9. Charged-current inelastic interaction of a muon neutrino in the BEBC bubble chamber filled with a liquid neon–hydrogen mixture. Along with the muon in the final state also hadrons have been formed, among them also neutral pions, whose decay products – two energetic photons – initiate electromagnetic cascades. The charged-particle tracks are bent in a 3.5 T magnetic field oriented perpendicular to the plane shown [19]; Photo credit CERN.

neutrino in the BEBC bubble chamber filled with a liquid neon–hydrogen mixture [19]. Along with the muon in the final state also hadrons have been formed, among them also neutral pions, whose decay products – two energetic photons – initiate electromagnetic cascades. The charged-particle tracks are bent in a 3.5 T magnetic field oriented perpendicular to the plane shown.

In recent times nuclear emulsions have been rejuvenated in the field of neutrino interactions. Nuclear emulsions provide μm resolution which is required for measurement and identification of ν_τ interactions. τ leptons with a $c\tau_\tau = 87\,\mu\text{m}$ require excellent spatial resolution for their identification, because not only the production vertex, but also the decay

https://doi.org/10.1017/9781009401531.013 Published online by Cambridge University Press

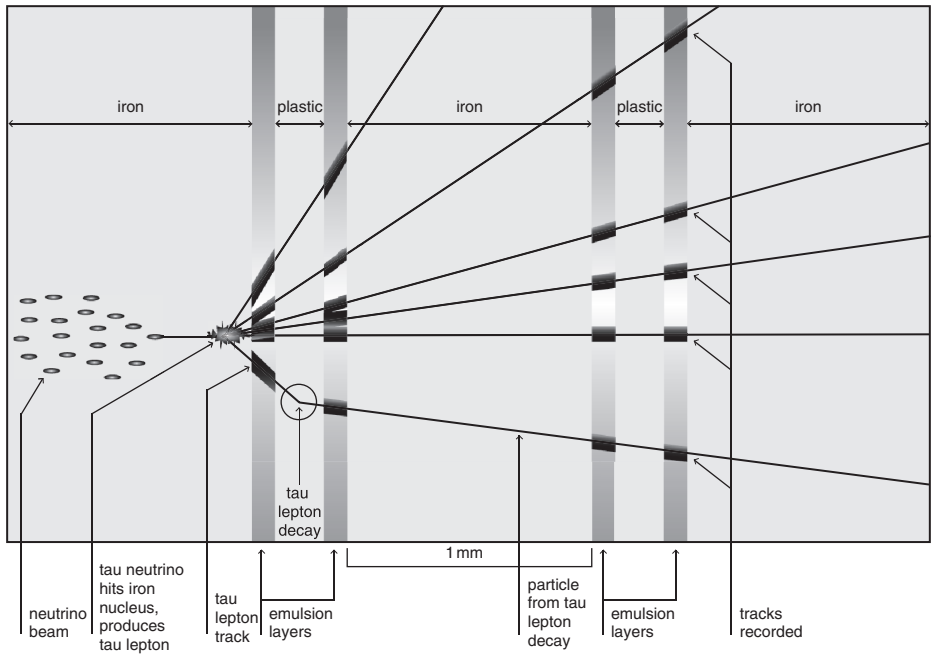

Fig. 10.10. Schematics of the ν_τ detection; illustration courtesy of Fermilab Experiment E872, Direct Observation of Nu Tau [20]. Of one billion*(10^{12}) tau neutrinos crossing the DONUT detector, only about one is expected to interact with an iron nucleus.

vertex must be unambiguously identified. Figures 10.10 and 10.11 show the schematics of the ν_τ detection and a real event in the DONUT experiment [20, 21]. The reconstructed event display shows different projections of the ν_τ interaction.

The detection of solar neutrinos or neutrinos from supernova explosions has been performed in large water Cherenkov detectors. In these detectors only ν_e or $\bar{\nu}_e$ can be measured because solar or SN neutrinos have insufficient energy to create other lepton flavours. Typical reactions are

$$\nu_e + e^- \rightarrow \nu_e + e^- \tag{10.36}$$

or

$$\bar{\nu}_e + p \rightarrow e^+ + n \ , \tag{10.37}$$

where the final-state electron or positron is detected.

If higher-energy neutrinos are available, such as from interactions of primary cosmic rays in the atmosphere and the decay of pions and kaons, one

* Beware: the European 'billion' is 10^{12} in contrast to an American 'billion', which is just 10^9.

https://doi.org/10.1017/9781009401531.013 Published online by Cambridge University Press

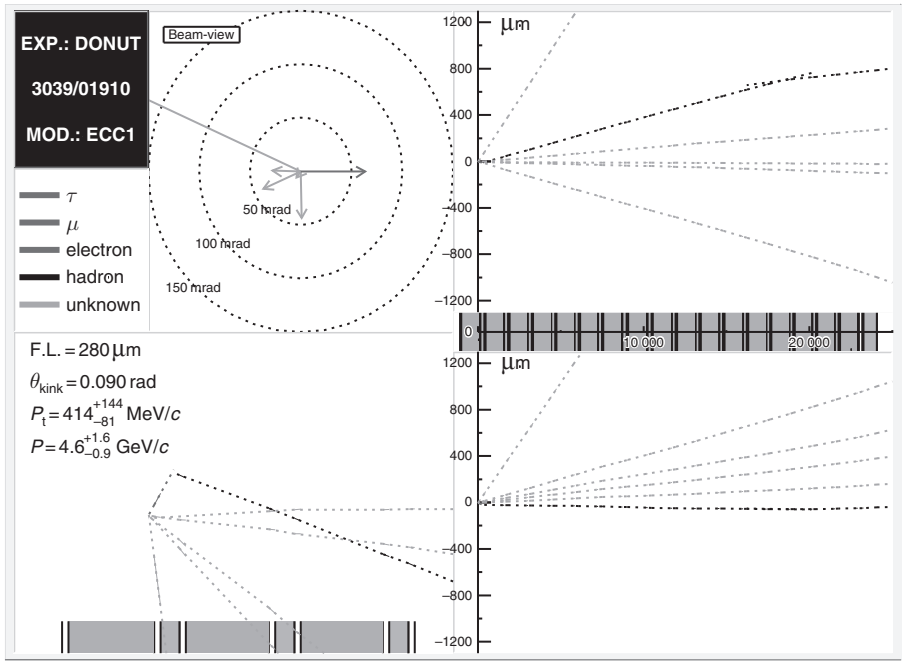

Fig. 10.11. Detection of the τ neutrino in the DONUT experiment; illustration courtesy of Fermilab Experiment E872, Direct Observation of Nu Tau [21].

can produce energetic electrons and muons which can easily be identified in large-volume water Cherenkov counters. The Cherenkov light produced by the charged final-state particles is measured by a large assembly of photomultipliers, where a substantial coverage of the detector end faces eases energy measurements and spatial reconstruction. Figure 10.12 shows the large-volume water Cherenkov counter SuperKamiokande with its central detector surrounded by an anticoincidence shield which vetoes remnant charged particles produced in the atmosphere [22].

Figures 10.13 and 10.14 show signatures of an electron and a muon produced in an electron-neutrino and muon-neutrino interaction, respectively [22]. The barrel part of the SuperKamiokande detector has been unwrapped, and the lower and the upper circular part of the cylindrically shaped detector has been added in the appropriate place. Electrons initiate electromagnetic showers in the water. Therefore their Cherenkov pattern shows some fuzziness at the edges of the Cherenkov ring, while muons do not start showers leading to a clear, distinct Cherenkov pattern.

Because of the large background from atmospheric neutrinos, the detection of neutrinos from cosmic-ray sources in our galaxy and beyond is limited to the TeV region. The expected flux of such neutrinos is low, so

https://doi.org/10.1017/9781009401531.013 Published online by Cambridge University Press

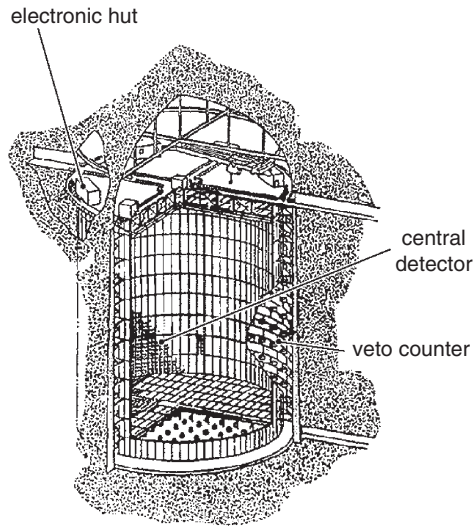

Fig. 10.12. Sketch of the SuperKamiokande detector [22].

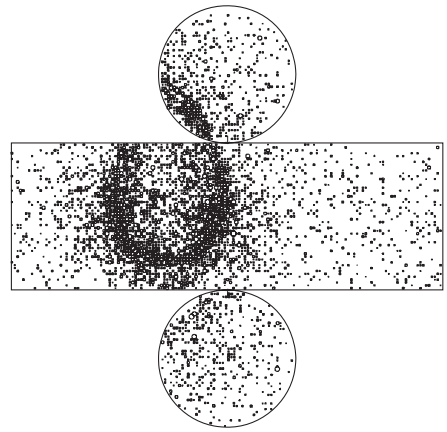

Fig. 10.13. Signature of an electron in the SuperKamiokande experiment [22].

huge detectors must be provided. Large-volume water or ice Cherenkov detectors (Baikal, AMANDA, IceCube, ANTARES, NESTOR or NEMO) are being prepared or are taking data already. The measurement principle is the detection of energetic muons produced in $\nu_\mu N$ interactions, where in the TeV region the energy loss of muons by bremsstrahlung and direct electron-pair production – being proportional to the muon energy – provides calorimetric information. Figure 10.15 shows the layout of the AMANDA-II detector in the antarctic ice at the South Pole [23], and Fig. 10.16 is an example of an upgoing muon produced by a

https://doi.org/10.1017/9781009401531.013 Published online by Cambridge University Press

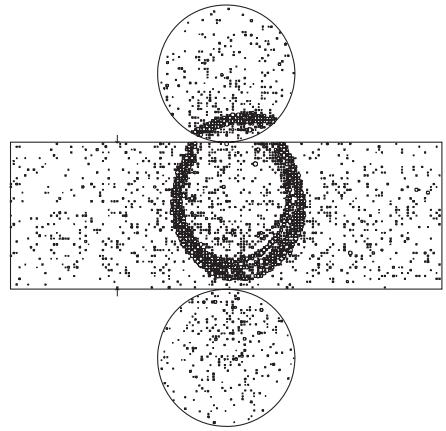

Fig. 10.14. Signature of a muon in the SuperKamiokande experiment [22].

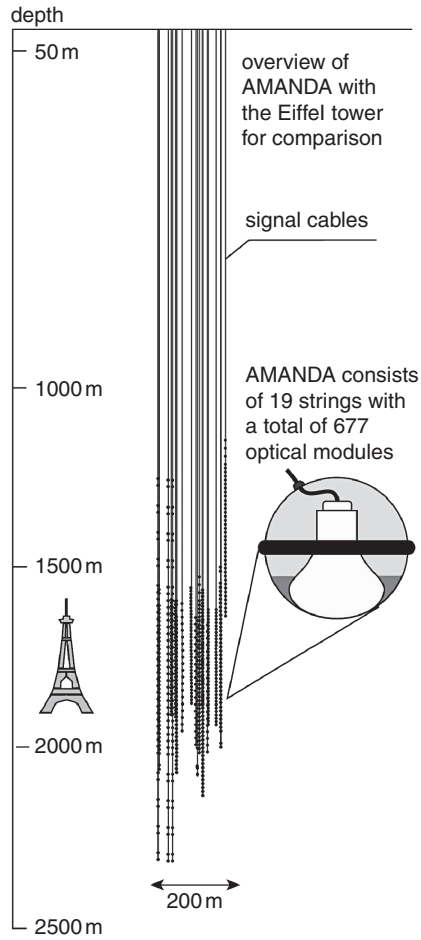

Fig. 10.15. Sketch of the AMANDA-II array at the South Pole [23].

https://doi.org/10.1017/9781009401531.013 Published online by Cambridge University Press

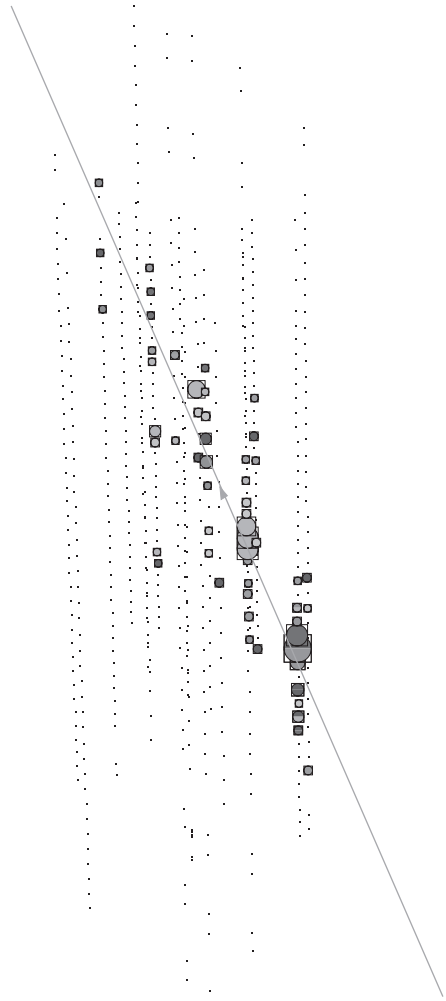

Fig. 10.16. Event display of a neutrino-induced upward-going muon [24].

cosmic-ray neutrino in a muon-neutrino interaction [24]. Until now the operating large-volume water and ice Cherenkov detectors have only seen atmospheric ν_μ neutrinos.

The observation and measurement of blackbody photons in the microwave band has provided important cosmological information on the structure and evolution of the universe. The measurement of Big Bang neutrinos which have energies comparable to those of 2.7 K microwave photons presents a challenge to detector builders. At the moment no technique is conceivable how to detect these primordial neutrinos in the MeV range.

https://doi.org/10.1017/9781009401531.013 Published online by Cambridge University Press

Neutrino physics is mostly an issue at accelerators, in cosmic rays or with reactor experiments. Now that neutrino propagation in the framework of neutrino oscillations is understood [25], neutrinos can also be used as probes, e.g., to search for oil or hydrocarbons in the Earth's crust, to investigate the inner part of the Earth, or to help to clarify the question of the radiogenic contribution to the terrestrial heat production by measuring geoneutrinos from the decay of the naturally occurring radioisotopes uranium (^{238}U), thorium (^{232}Th) and potassium (^{40}K).

10.5 Problems

10.1 The Sun converts protons into helium according to the reaction

$$4p \;\rightarrow\; {}^4\mathrm{He} + 2e^+ + 2\nu_e \;.$$

The solar constant describing the power of the Sun at Earth is $P \approx 1400\,\mathrm{W/m^2}$. The energy gain for this fusion reaction of 26.1 MeV differs slightly from the binding energy of helium ($E_\mathrm{B}(^4\mathrm{He}) = 28.3\,\mathrm{MeV}$), because the neutrinos produced in this chain also take some energy. How many solar neutrinos arrive at Earth?

10.2 If solar electron neutrinos oscillate into muon or tau neutrinos they could in principle be detected via the reactions

$$\nu_\mu + e^- \;\rightarrow\; \mu^- + \nu_e \;, \quad \nu_\tau + e^- \;\rightarrow\; \tau^- + \nu_e \;.$$

Work out the threshold energy for these reactions to occur. (Assume that the target electrons are at rest.)

10.3 Radiation exposure due to solar neutrinos. Use

$$\sigma(\nu_e N) \approx 10^{-45}\,\mathrm{cm^2/nucleon}$$

to work out the number of interactions of solar neutrinos in the human body (tissue density $\varrho \approx 1\,\mathrm{g/cm^3}$). Neutrinos interact in the human body by

$$\nu_e + N \;\rightarrow\; e^- + N' \;,$$

where the radiation damage is caused by the electrons. Estimate the annual dose for a human under the assumption that on average 50% of the neutrino energy is transferred to the electron. The equivalent dose is defined as

$$H = (\Delta E/m)\, w_R$$

https://doi.org/10.1017/9781009401531.013 Published online by Cambridge University Press

(m is the mass of the human body, w_R the radiation weighting factor (= 1 for electrons), $[H] = 1\,\mathrm{Sv} = 1\,w_R\ \mathrm{J/kg}$, and ΔE the energy deposit in the human body). Work out the annual equivalent dose due to solar neutrinos and compare it with the normal dose due to natural radiation from the environment of $H_0 \approx 2\,\mathrm{mSv/a}$.

10.4 Work out the muon and neutrino energies in pion and leptonic kaon decay at rest ($\pi^+ \to \mu^+ + \nu_\mu$, $K^+ \to \mu^+ + \nu_\mu$).

10.5 Two electron neutrinos with energies E_1 and E_2 and an assumed rest mass m_0 are emitted from the supernova 1987A at exactly the same time. What is their arrival-time difference at Earth (distance to SN 1987A is r), and how can their mass be inferred from such a time-difference measurement if $m_0c^2 \ll E$ is assumed for the neutrino?

10.6 It is considered realistic that a point source in our galaxy produces a neutrino spectrum according to

$$\frac{\mathrm{d}N}{\mathrm{d}E_\nu} = 2 \cdot 10^{-11}\,\frac{100}{E_\nu^2\,[\mathrm{TeV}^2]}\,\mathrm{cm}^{-2}\,\mathrm{s}^{-1}\,\mathrm{TeV}^{-1}\ . \tag{10.38}$$

This leads to an integral flux of neutrinos of

$$\Phi_\nu(E_\nu > 100\,\mathrm{TeV}) = 2 \cdot 10^{-11}\,\mathrm{cm}^{-2}\,\mathrm{s}^{-1}\ . \tag{10.39}$$

Work out the annual interaction rate of $> 100\,\mathrm{TeV}$ neutrinos in IceCube ($d = 1\,\mathrm{km} = 10^5\,\mathrm{cm}$, $\varrho(\mathrm{ice}) \approx 1\,\mathrm{g/cm}^3$, $A_{\mathrm{eff}} = 1\,\mathrm{km}^2$).

References

[1] John N. Bahcall, *Neutrino Astrophysics*, Cambridge University Press, Cambridge (1989)

[2] H.V. Klapdor-Kleingrothaus & K. Zuber, *Particle Astrophysics*, Institute of Physics Publishing, Bristol (2000)

[3] H.V. Klapdor-Kleingrothaus & K. Zuber, *Teilchenphysik ohne Beschleuniger*, Teubner, Stuttgart (1995)

[4] J.A. Peacock, *Cosmological Physics*, Cambridge University Press, Cambridge (1999)

[5] P. Adhya, D.R. Chaudhuri & S. Hannestad, Late-Time Entropy Production from Scalar Decay and the Relic Neutrino Temperature, *Phys. Rev.* **D68** (2003) 083519, 1–6

[6] F. Reines, C.L. Cowan, F.B. Harrison, A.D. McGuire & H.W. Kruse (Los Alamos), Detection of the Free Antineutrino, *Phys. Rev.* **117** (1960) 159–73; C.L. Cowan, F. Reines, F.B. Harrison, H.W. Kruse & A.D. McGuire

(Los Alamos), Detection of the Free Neutrino: A Confirmation, *Science* **124** (1956) 103–4

[7] G. Danby, J.M. Gaillard, K. Goulianos, L.M. Lederman, N. Mistry, M. Schwartz & J. Steinberger (Columbia U. and Brookhaven) 1962, Observation of High Energy Neutrino Reactions and the Existence of Two Kinds of Neutrinos, *Phys. Rev. Lett.* **9** (1962) 36–44

[8] M. Perl *et al.*, Evidence for Anomalous Lepton Production in $e^+ - e^-$ Annihilation, *Phys. Rev. Lett.* **35** (1975) 1489–92

[9] K. Kodama *et al.*, Detection and Analysis of Tau-Neutrino Interactions in DONUT Emulsion Target, *Nucl. Instr. Meth.* **A493** (2002) 45–66

[10] J.N. Bahcall & R. Davis Jr, *Essays in Nuclear Astrophysics*, Cambridge University Press, Cambridge (1982)

[11] R. Davis Jr, *A Half Century with Solar Neutrinos, Nobel Lecture, from 'Les Prix Nobel'*, ed. T. Frängsmyr, Stockholm (2003)

[12] R. Wink *et al.*, The Miniaturised Proportional Counter HD-2(Fe)/(Si) for the GALLEX Solar Neutrino Experiment, *Nucl. Instr. Meth.* **A329** (1993) 541–50; www.mpi-hd.mpg.de/nuastro/gallex/counter.gif

[13] W. Hampel, private communication (2006)

[14] CERN–Dortmund–Heidelberg–Saclay Collaboration (J. Knobloch *et al.*) 1981, In Wailea 1981, Proceedings, Neutrino '81, Vol. 1, 421–8, http://knobloch.home.cern.ch/knobloch/cdhs/cdhs.html; and private communication by J. Knobloch

[15] KARMEN Collaboration (W. Kretschmer for the collaboration), Neutrino Physics with KARMEN, *Acta Phys. Polon.* **B33** (2002) 1775–90; www-ik1.fzk.de/www/karmen/karmen_e.html

[16] NOMAD Collaboration (A. Cardini for the collaboration), The NOMAD Experiment: A Status Report, Prepared for 4th International Workshop on Tau Lepton Physics (TAU 96), Estes Park, Colorado, 16–9 September 1996, *Nucl. Phys. B Proc. Suppl.* **55** (1997) 425–32; http://nomadinfo.cern.ch/

[17] H.P. Reinhard (CERN), First Operation of Bebc, in Frascati 1973, Proceedings, High Energy Instrumentation Conference, Frascati 1973, 87–96; and *Status and Problems of Large Bubble Chambers*, Frascati 1973, 3–12; www.bo.infn.it/antares/bolle_proc/foto.html; http://doc.cern.ch/archive/electronic/cern/others/PHO/photo-hi/7701602.jpeg; Photo credit CERN

[18] www.anl.gov/OPA/news96arch/news961113.html

[19] W.S.C. Williams, *Nuclear and Particle Physics*, Clarendon Press, Oxford (1991)

[20] www.fnal.gov/pub/inquiring/physics/neutrino/discovery/photos/signal_low.jpg

[21] www-donut.fnal.gov/web_pages/

[22] T. Kajita & Y. Totsuka, Observation of Atmospheric Neutrinos, *Rev. Mod. Phys.* **73** (2001) 85–118

[23] AMANDA Collaboration (K. Hanson *et al.*), July 2002, 3pp., Prepared for 31st International Conference on High Energy Physics (ICHEP 2002), Amsterdam, The Netherlands, 24–31 July 2002, Amsterdam 2002, ICHEP

126–8; http://amanda.uci.edu/; and private communication by Chr. Spiering (2003), Chr. Walck & P.O. Hulth (2007)
[24] AMANDA Collaboration, Christian Spiering, private communications (2004)
[25] S.M. Bilenky & B. Pontecorvo, Lepton Mixing and Neutrino Oscillations, *Phys. Rep.* **41** (1978) 225–61